Journal of Bioresources and Bioproducts 7 (2022) 99–108

Contents lists available at ScienceDirect

Journal of Bioresources and Bioproducts

journal homepage: http://www.keaipublishing.com/en/journals/journal-of-bioresources-and-bioproducts/

A mixed acid methodology to produce thermally stable cellulose nanocrystal at high yield using phosphoric acid

Khairatun Najwa Mohd Amin[a,b,*], Alireza Hosseinmardi[a], Darren J. Martin[a], Pratheep K. Annamalai[a,*]

[a] *Australian Institute for Bioengineering and Nanotechnology (AIBN), the University of Queensland, Brisbane, QLD 4072 Australia*
[b] *Faculty of Chemical and Process Engineering Technology, College of Engineering Technology, Universiti Malaysia Pahang, Lebuhraya Tun Razak, 26300 Gambang Kuantan, Pahang D.M. Malaysia*

ARTICLE INFO

Keywords:
Cellulose nanocrystal (CNC)
Acid hydrolysis
Thermal stability
Mixed acid
Crystallinity
Production yield

ABSTRACT

Cellulose nanocrystal (CNC) with distinctive shape-morphology, enhanced thermal stability and dispersibility is essential for overcoming the challenges in processing polymer/CNC nanocomposites through melt compounding at elevated temperatures. This study shows a mixed acid hydrolysis method to produce CNC with improved thermal stability and high productivity. The use of phosphoric acid (H_3PO_4), as a mild acid, in combination with a strong acid either sulphuric acid (H_2SO_4) or hydrochloric acid (HCl) leads to reduced use of strong acids and low impact on our environment. The influences of acid combination and sequence of addition on the production yield were investigated by retaining the proportion of H_3PO_4 to corrosive acid (H_2SO_4 and HCl) 4 to 1, and solid to liquid ratio 1:75. This methodology has enabled to isolate CNC with higher thermal stability, dispersibility and productivity in terms of amount acid used 1 g of CNC, as compared with single acid hydrolysis. The CNC produced using the combination of H_3PO_4 and HCl exhibits high thermal stability, dispersibility and rod-like shape morphology with length and width of (424 ± 86) and (22 ± 3) nm, respectively. Moreover, this approach has reduced H_3PO_4 consumption by 54% as compared with single acid hydrolysis method for the production of same amount of CNC.

1. Introduction

Cellulose nanocrystal (CNC), a biobased sustainable nanomaterial with versatile morphology and surface functionalities can be derived from plants like jute (Bashar et al., 2019), cotton (Jordan et al., 2019) and wood (Beck-Candanedo et al., 2005), sea creatures like tunicates (Dunlop et al., 2018) as well as bacteria (Sperotto et al., 2021). The combination of good mechanical properties, low toxicity and renewable origin makes CNC as the most auspicious nanoscale material for future engineering applications (Moon et al., 2011). Recently, notable reinforcement effect by CNC in numerous polymer matrices such as polypropylene (Bagheriasl et al., 2015; Nagalakshmaiah et al., 2017; Sojoudiasli et al., 2018), polyethylene (Gray et al., 2018; Hendren et al., 2020), polyamide (Rahimi and Otaigbe 2017; Reid et al., 2019), polyvinyl alcohol (Roohani et al., 2008; Fan et al., 2019)) has been reported. The CNC/polymer nanocomposites have showed improved mechanical properties at very low loadings (< 5% V/V) without compromising optical requirements (Mendez et al., 2011; Pei et al., 2011). These CNC/polymer nanocomposites can be implemented in various applications like protective gears, paints, drug carrier, automotive, filtration and textiles (Hamdan et al., 2021; Norrrahim et al., 2021). The importance of the production of CNC comes not only from the remarkable improvements in properties and new functional

* Corresponding authors.
E-mail addresses: knajwa@ump.edu.my (K.N.M. Amin), p.annamalai@uq.edu.au (P.K. Annamalai).

https://doi.org/10.1016/j.jobab.2021.12.002
Received 20 July 2021; Received in revised form 1 December 2021; Accepted 8 December 2021
Available online 8 January 2022

properties, but it also adds value to the broader biorefinery of plant biomass (paper pulp, agricultural residue, food waste) in terms of economic and environmental benefits.

The CNC/polymer nanocomposites can be fabricated through four different methods, solution casting, in-situ polymerisation, organo-gel template method and melt compounding (Miao and Hamad, 2019). The best technique preferred at the industrial scale for environmental and economic reasons, is melt compounding or extrusion due to significant reduction of solvent usage (Amin et al., 2016). However, the reinforcement potential of CNC in the nanocomposites has been limited due to its poor thermal properties. Thus to enhance the melt-processibility of CNC with polymers, surface modification of CNC by esterification (Li et al., 2017; Leszczyńska et al., 2018), organic compatibiliser (Ben Azouz et al., 2012; Lin and Dufresne, 2013) and grafting (Lin and Dufresne, 2013) have been adopted to improve their thermal stability. Generally, the rod-like CNC is produced via acid hydrolysis, enzymatic, ultra-sonication, or mechanical treatments (Mohd Amin et al., 2015). The most common method is sulphuric acid hydrolysis (Mendez et al., 2011; Annamalai et al., 2014; Chen et al., 2015) as it produces CNC with well dispersion in most polymers and polar solvents. However, sulphate groups $(SO_4)^{2-}$ present on the surface of CNC may cause degradation via dehydration thus causing poor thermal stability (Molnes et al., 2017; Wang et al., 2007). With the aims to produce enhanced thermal stability CNC, a few techniques have been made through mechanical and sono-chemical shearing (Filson and Dawsondoh, 2009; Li et al., 2012; Mohd Amin et al., 2015), ionic liquid-treatment (Lazko et al., 2014; Song et al., 2018), resin-catalysed hydrolysis (Tang et al., 2011) methods and the typical acid hydrolysis method using other mild acids like phosphoric acid (Camarero Espinosa et al., 2013), mineral acids such as HCl (Yu et al., 2013; Mahmud et al., 2019), and formic acid (Sun et al., 2008). Hydrochloric acid hydrolysis can produce CNC with high thermal stability, however, it tends to flocculate in the aqueous suspensions (Corrêa et al., 2010; Rosa et al., 2010). Meanwhile, the acid hydrolysis using phosphoric and formic acids, consumed significantly high volume of acid based on the ratio between production yield and raw materials (Kupiainen et al., 2012; Camarero Espinosa et al., 2013; Vanderfleet et al., 2019). Moreover, the phosphoric acid tends to decrease the crystallinity of cellulose (Vinogradov et al., 2002; Jia et al., 2013; Hirayama et al., 2020). On the other hand, the idea of employing of acid mixtures for hydrolysis, was developed in order to produce thermally stable CNC, for example, mixed sulphuric/oxalic acid (Xie et al., 2019), sulphuric/phosphoric acid (Vanderfleet et al., 2019) and HCl/citric acid (Yu et al., 2019). However, the production yield of the resulting CNC is not as high as the single acid hydrolysis system.

The aim of this study is to develop a high production-yield approach to produce, thermally stable CNC, suitable for melt mixing, while reducing the environmental hazards of using of acid. Therefore, reduction in overall consumption of phosphoric acid was investigated. In addition, we studied the combined effect of phosphoric acid (i.e., improvement in thermal stability of resultant CNC) with a strong acid either hydrochloric acid or sulphuric acid (i.e., hydrolytic reaction). Herein, by performing the acid hydrolysis in two sequences of addition of two acids, we reported the production of thermally stable CNC with retained crystallinity and distinctive shape morphology using remarkably reduced amount of acids thereby subsequently lowering the environmental impact.

2. Experimental

2.1. Materials

Microcrystalline cellulose (MCC) (Avicel PH-101) powder (~100% pure) was used as received from FMC BioPolymer Corporation.ionic. Three kinds of acids were used for hydrolysis which were hydrochloric acid (32%) purchased from Ajax Finechem Pty. Ltd., meanwhile ortho-phosphoric acid (85%) and sulphuric acid (98%) were bought from Merck.

2.2. Acid hydrolysis of MCC

2.2.1. Single acid

The acid hydrolysis of MCC using phosphoric acid (H_3PO_4) was adapted from (Camarero Espinosa et al., 2013) with slight modification at optimised conditions (Fig. S1 and Table S1 in Supplementary Materials) with a solid (wt) to liquid (V) ratio of 1 to 75 and at a concentration of H_3PO_4 around 63% (wt/V). Briefly, the MCC powder was dispersed in deionised water at room temperature. To this mixture under ice-bath cooling, H_3PO_4 was gradually added dropwise over 15 min under mild stirring (200 r/min) and then the mixture was heated to 70 °C. After 30 min digestion at 70 °C under vigorous stirring (700 r/min) and was cooled to room temperature. Then it was centrifuged (for 4–5 times at 4750 r/min), dialysed (with a tubing of molecular weight cut-off 14 000) in deionised water, ultrasonication and freeze-drying processes. For comparison on thermal stability, the hydrolysis was also carried out with H_2SO_4 at same solid to liquid ratio, a concentration of 32% (wt/V) and at 50 °C for 3.5 h following a reported protocol (Bondeson et al., 2006). The CNCs obtained from hydrolysis using H_3PO_4 and H_2SO_4 are denoted as CNC-P and CNC-S, respectively.

2.2.2. Mixed acid

In the mixed acid methodology, partial substitution of the phosphoric acid (pK_{a1}~2.14) with strong acid (H_2SO_4 (pK_{a1}~ –3.0), HCl (pKa~ –6.3)) has allowed us to reduce the time and temperature for the hydrolysis. Keeping the volume ratio of mild acid (H_3PO_4) to strong acid (H_2SO_4, HCl) as 4:1 constant at the same solid to total liquid ratio (1:75) as above, the hydrolysis was carried out via two sequences of acid addition (Fig. S2 in Supplementary Materials). In the first route, 5.2 g of MCC dispersed in 200 mL deionised water was hydrolysed with H_3PO_4 (85%, 150 mL) for 1.5 h at 50 °C. Then, sulphuric acid (98%, 40 mL) was added and reacted for 1 h. In the second route, the hydrolysis was first done with H_2SO_4 for 1 h followed by H_3PO_4 for another 1.5 h, while keeping the amount of acids constant. Subsequently, the suspension was further processed through centrifugation, dialysis and ultrasonication steps as described for the single acid hydrolysis method. For comparison, the mixed acid hydrolysis was performed similarly in combination of

H_3PO_4 and HCl. The CNCs obtained were labelled as CNC-*XY* where *X* designates as the first acid and *Y* denotes the second acid such as sulphuric acid (S), hydrochloric acid (H) or phosphoric acid (P). For example, the sample CNC-PH represents that the hydrolysis was performed by adding H_3PO_4 first and HCl second.

2.3. Characterisation

The production yield was calculated from the dry weight of CNC (solid content) obtained after freeze-drying, with respect to the dry weight of raw material used. It is also further interpreted as the required volume of concentrated acids to produce 1 g of CNC. The structure and the aspect ratio of the CNC was determined using transmission electron microscopy (TEM). The 2% aqueous uranyl acetate was used to stain the grids and was analysed. The dimensions (length and width of CNC) were estimated using ImageJ software with at least 10 particles in TEM images.

Thermogravimetric analysis (TGA) measurements were performed using Mettler Toledo DSC/TGA Star system. In nitrogen atmosphere, initially, with heating rate of 10 °C/min, the samples were heated from 25 °C to 110 °C. Then, it was isothermally held for 10 min and subsequently heated to 500 °C with rate of 5 °C/min.

To determine crystallinity of CNC, X-ray diffraction (XRD) was performed with scanning rate at 2°/min and step size of 0.02° in the range of $2\theta = 1°–40°$. The crystallinity index of CNC was determined by the XRD peak height method. The degree of crystallinity (%) was calculated using Equation (1):

$$I_{Cr} = \frac{I_{002} - I_{am}}{I_{002}} \times 100\% \quad (1)$$

where I_{002} is the maximum intensity of the peak corresponding to the plane having the miller indices of 002, and I_{am} is the minimal intensity of diffraction of the amorphous phase at $2\theta = 18°$.

The dispersibility of CNCs was studied by dispersing them in dimethylformamide (DMF) as well as deionised water. The photographs of the dispersions in sample vials were taken at different time intervals (1 h, 24 h and 10 d) after ultrasonication for 2 min. The zeta (ζ) potentials of the CNC were measured in deionised water at a concentration of 0.01 mg/mL with a Zetasizer analyser. Smoluchowski equation was used to calculate the ζ potential. The surface charge concentration of CNCs were determined using conductometric titrations. 50 mg of CNC was dispersed in a mixture of 10 mL HCl (0.01 mol/L) and 25 mL deionised water and was further sonicated for 10 min. The titration was performed with 0.01 mol/L sodium hydroxide (NaOH). Equation (2) was used to calculate the concentration of sulphate (SO_4^{2-}) and phosphate (PO_4^{3-}) groups (*C*):

$$C = \frac{SO_4^- / PO_4^- \text{ (mmol)}}{\text{cellulose (kg)}} = \frac{C_{NaOH} \times V_{NaOH}}{W_{CNC}} \times 10^6 \quad (2)$$

where W_{CNC} is the weight of CNC (g), V_{NaOH} and C_{NaOH} are the volume (L) and concentration (mol/L) of NaOH used.

3. Results and Discussion

3.1. Single acid method

Our preliminary investigation on the optimisation of the phosphoric acid hydrolysis conditions showed high yield for hydrolysis at 70 °C for 30 min (Fig. S1). Fig. 1 shows optical micrograph (OM) of MCC powder (a) compares the TEM images (b, c) and TGA thermogram (d) of CNC-P and the CNC obtained from H_2SO_4 hydrolysis (CNC-S) process. The CNC-P produced under this method exhibit rod-like shape and the sizes recorded length of 168 nm and diameter of 9.6 nm with an aspect ratio of 20. It is comparable to that of CNC-S which has dimensions of (244.5 ± 54) nm in length and (6.9 ± 1.5) nm in diameter with an aspect ratio of 35. Meanwhile, TGA analysis (Fig. 1d) shows improved thermal stability CNC-P with an onset degradation temperature at 280 °C as compared with MCC powder (270 °C) and CNC-S (237 °C).

3.2. Mixed acid method

Fig. 2 shows TEM images of CNCs isolated from mixed acid hydrolysis. These CNCs showed rod-like morphology similar that of CNCs obtained via single acid hydrolysis (i.e., CNC-S or CNC-P) indicating no/insignificant influence on CNC morphology by the mixture of acids. Table 1 summarises the dimensions (length distribution of CNCs is illustrated in Fig. S3) measured from TEM images with values obtained for production yield and degree of crystallinity (%).

Overall, the CNC produced via mixed acid hydrolysis recorded an average length varying between 360 nm and 400 nm and width varying between 16 nm and 22 nm and resulting in an aspect ratio in the range of 18–22. The values obtained were similar to the CNC produced via single acid (H_2SO_4 or H_3PO_4) hydrolysis (Bondeson et al., 2006; Capadona et al., 2007; Bai et al., 2009; Camarero Espinosa et al., 2013).

3.3. Production yield

The efficiency of mixed acid was rationalised in terms of production yield and the consumption of acid for one gram of resulting CNC. As compared with the CNC-P obtained via single acid method, the consumption of acids is reduced in the mixed acid method.

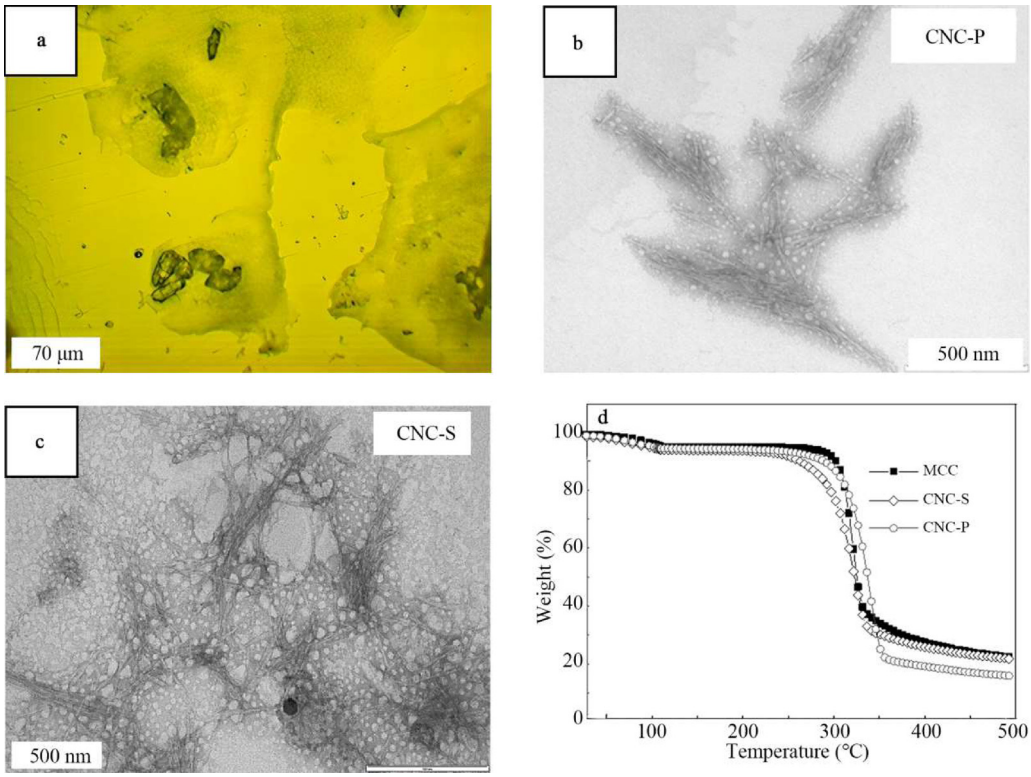

Fig. 1. Optical micrograph of microcrystalline cellulose (MCC) (a) and TEM (b, c) and TGA curve (d) of cellulose nanocrystal (CNC) isolated via phosphoric and sulphuric acid hydrolysis (CNC-P and CNC-S).

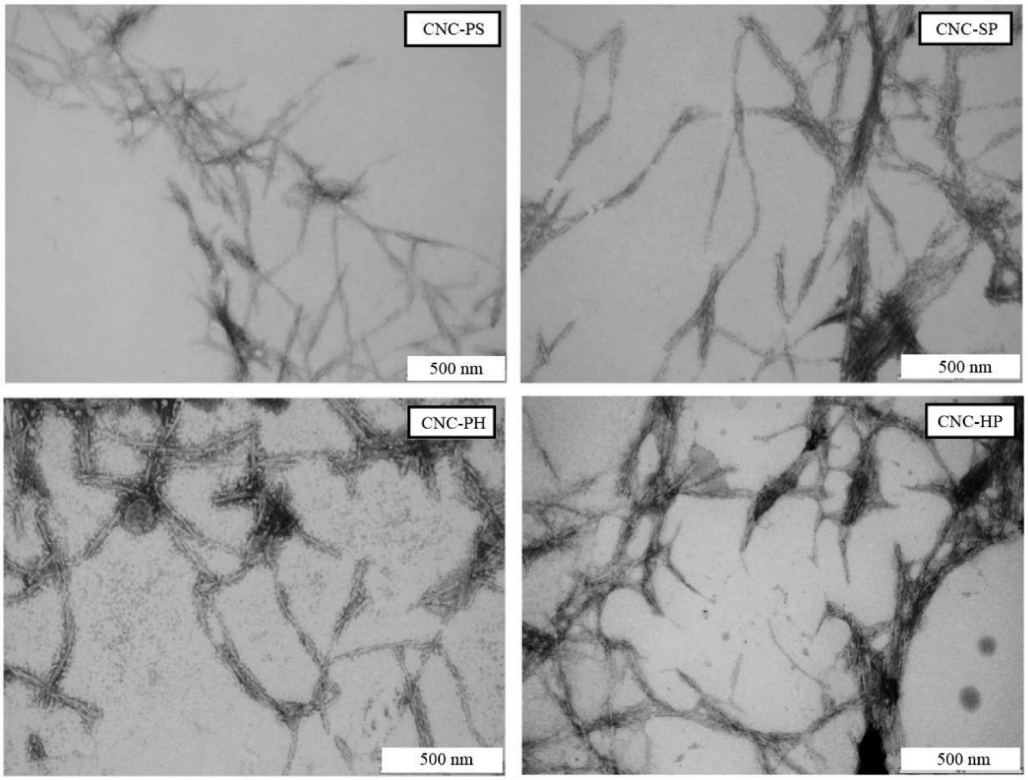

Fig. 2. Transmission electron microscopy (TEM) images of CNCs isolated via mixed acid hydrolysis.

Table 1
Dimensions, production yield and degree of crystallinity of CNC obtained through mixed acid hydrolysis.

Item	Length (nm)	Width (nm)	Aspect ratio	Production yield (%)	H_3PO_4 acid required for 1 g of CNC (mL)	H_2SO_4 or HCl acid required for 1 g of CNC (mL)	Degree of crystallinity (%)
CNC-P	168.6±18	9.6±4	20	85	64	–	91.2
CNC-PS	364.3±89	19.9±6	18	93	31	8	91.1
CNC-SP	368.4±99	20.8±7	18	98	29	8	89.7
CNC-PH	424.7±86	22.3±3	19	99	29	8	92.8
CNC-HP	363.2±109	16.6±3	22	101	29	8	93.2

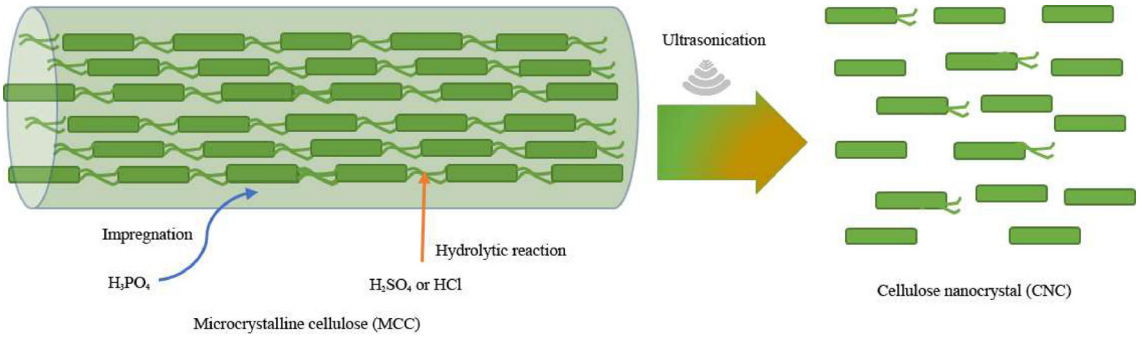

Fig. 3. Schematic representation of potential components involved in mixed acid hydrolysis method.

For example, in case of CNC-PH, a remarkable reduction of H_3PO_4 was successfully achieved up to 54% with respect to the acid required for producing 1 g of CNC, when combined with HCl acid. This can be attributed to potential synergistic effect (hydrolytic reaction and swelling) of two acids. As schematically represented in Fig. 3, the strong acid contributes well to the hydrolytic reaction as they have higher (proton) dissociation capabilities than H_3PO_4, while the H_3PO_4 contributes to the penetration and swelling of cellulose.

Hence the first 1 h mixing of cellulose in H_3PO_4 at low concentration (32wt%) enables the impregnation, swelling of nanocrystal aggregates present in MCC (Boerstoel et al., 2001; Zhang et al., 2006; 2009) and further treatment with H_2SO_4 (10wt%) or HCl (3.7wt%) enables further disassociation of nanocrystal aggregates by promoting hydrolytic reactions and breaking hydrogen bonding between the nanocrystals. In case of the process with H_2SO_4, the surface of CNC will be left with residual sulphate groups, while promoting the hydrolysis (Roman and Winter 2004; Kupiainen et al., 2012) and resulting CNC with relatively a low yield. In case of the process with HCl (at low concentration), the promotion of hydrolytic reaction is relatively lower as compared to H_2SO_4. The differences in actions (hydrolysis vs impregnation) and sequence of addition of acid exhibit the implications on the crystallinity of the CNC obtained.

Notably, the CNC-HP achieved a high production yield of 101% (slightly higher than the initial raw material). The reason is unknown at this stage, but can be attributed to a slight weight increase due to phosphorylation or incomplete removal of swollen domains of cellulose. Also, both the hydrochloric and phosphoric acids are less corrosive than sulphuric acid (Boerstoel et al., 2001; Zhang et al., 2006).

3.4. Crystallinity

All the samples (MCC and CNCs) have exhibited the characteristic peaks of crystalline polymorph I of cellulose at $2\theta = 15^\circ$ (101), 16.5° $(10\bar{1})$, 20.8° (021), 22.5° (002) and 34.3° (040) (Fig. S4). It shows that retained crystalline structure of cellulose that was observed for MCC at $2\theta = 22^\circ$ with a background peak for amorphous domains at $2\theta = 18^\circ$ (Segal et al., 1959; Hosseinmardi et al., 2018). The degree of crystallinity (%) values calculated from the peak cellulose I polymorph 22.5° (002) and peak for amorphous domains ($2\theta = 18^\circ$) in XRD patterns of the samples can be seen in Table 1. The crystallinity index for MCC powder before the hydrolysis was ~95% which is in the vicinity of reported values in the literature (Wei et al., 1996; Mohd Amin et al., 2015). After the hydrolysis through single acid, it is slightly reduced to 91.2%. This slight reduction is observed for mixed acid method as well, up to 91.1%, 89.7%, 92.8% and 93.2% for CNC-PS, CNC-SP, CNC-PH and CNC-HP, respectively. However, these values are still closer to that the most of CNCs isolated by single acid hydrolysis reported in the literature 60%–80% (Yue et al., 2012; Kargarzadeh et al., 2012) with the highest degree of crystallinity (91%) achieved through hydrobromic acid hydrolysis by Sadeghifar et al., (2011). Overall, the crystal structure in the cellulose was able to retain by using the mix acid hydrolysis process.

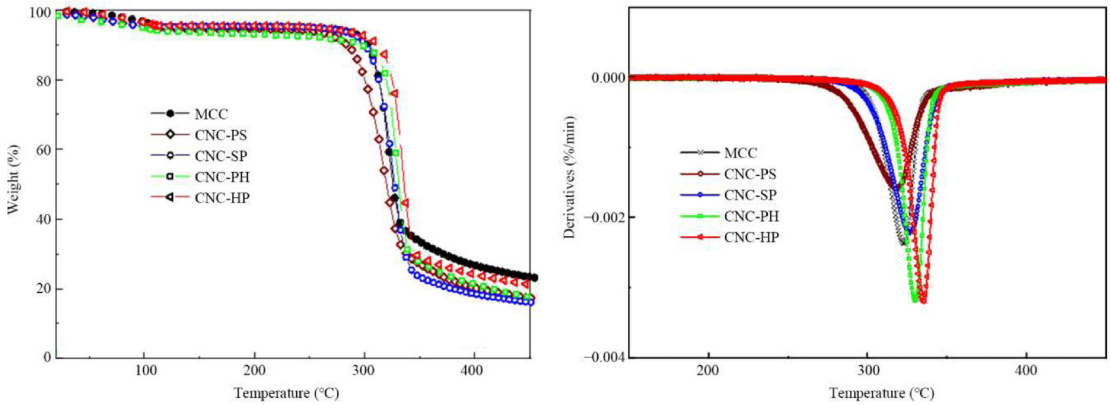

Fig. 4. Thermogravimetric analysis (TGA) curves and derivatives of MCC and CNC obtained from mixed acid hydrolysis.

Table 2
Degradation temperature and enthalpy for CNC obtained from mixed acid hydrolysis calculate from TGA curves.

Item	T_{onset} (°C)	Enthalpy (J/(g•°C)
CNC-PS	250	22.7
CNC-SP	274	27.8
CNC-PH	280	18.1
CNC-HP	295	12.5

3.5. Thermal stability

Fig. 4 shows thermal analysis of CNC produced via mixed acid hydrolysis. Lower onset degradation temperatures were recorded by CNC-PS and CNC-SP at 254 °C and 277 °C respectively than that observed for MCC. The lower thermal stability can be attributed to the degradation catalysed by sulphate groups $(SO_4)^{2-}$ introduced after hydrolysis.

Taking into account, these temperatures are better prior to values that testified onset degradation temperatures at 140 °C (Rämänen et al., 2012) and ~260 °C (Moon et al., 2011).

Besides, good thermal stability was also demonstrated by CNC-PH and CNC-HP at onset degradation temperature of 280–295 °C which is slightly lower than temperature achieved by Yu et al., (2013) at 300 °C where CNC isolated by HCl hydrolysis facilitated with hydrothermal conditions. Referring to the derivatives of TGA traces, broader peak ranged from ca. 260 °C to 350 °C can be observed and one distinct pyrolysis process was identified for CNCs isolated via mixed acid hydrolysis comprising sulphuric acid which indicates the presence of low content of the sulphate group (Wang et al., 2007). Meanwhile, CNCs isolated from combination of phosphoric and hydrochloric acids showed narrower derivative peaks with range from ca. 290 °C to 350 °C. This enhanced thermal stability can be attributed to the phosphorylation (with phosphate surface charges). The free hydroxyl groups and phosphate groups, in comparison with sulphate groups, do not promote dehydration reactions at low temperature regime. The influence of sequence of addition of acids was also observed as a modest improvement in thermal stability when the phosphoric acid was added second. Further investigation into the thermal degradation behaviour of CNCs was done by determination of enthalpy (calculated by area under the curve of TGA derivative peak) at the initial degradation point of the sample as listed in Table 2.

Obviously, the higher enthalpy values for CNC-PS or CNC-SP than CNC-PH or CNC-HP might support the catalytic effect of sulphate groups present in the CNC for the degradation of cellulose (Roman and Winter 2004). This is also confirmed by the lower char yield (15%–20%) for all CNC samples as compared with MCC (21%).

3.6. Dispersion of CNC

The ability to disperse well in the medium or matrix used is one of the main key features of good nano filler. Fig. 5 despites the fact that it was hard to distinguish the dispersion level between the CNCs, apparently all of them dispersed well in deionised water for 24 h and gradually flocculated after 10 d.

Meanwhile, CNC shows good dispersion in DMF after ultrasonication, but started to sediment after 1 h almost flocculated within 24 h. The better dispersibility in water might be occurred due to the hydrophilicity of CNC which tends to associate through strong hydrogen bonding with water molecules thus contributes good stability in aqueous suspension. However, in DMF which is less polar organic solvent, CNC propose a major aggregation of the suspended particles (Viet et al., 2007).

To gain further insight, zeta potential value was calculated to measure suspension stability in deionised water (Table 3). Almost similar values between 33 mV and 38 mV were recorded for all CNCs. Similar to the physical appearance pattern, this indicates

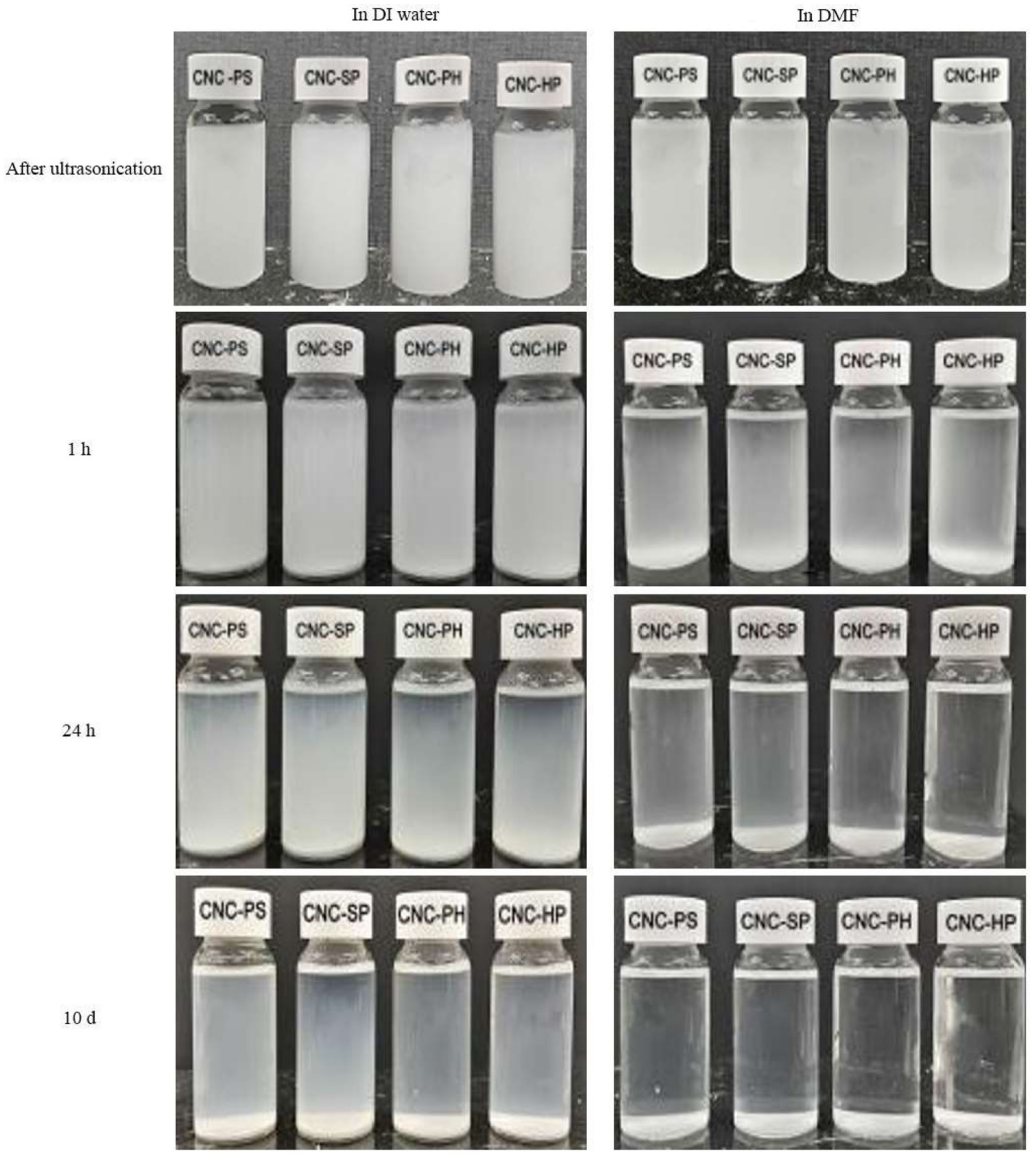

Fig. 5. Picture of CNCs taken after ultrasonication, 1 h, 24 h and 10 d in deionised (DI) water and dimethylformamide (DMF).

Table 3
Elemental analysis, zeta potential and number of charges of CNCs.

Item	Zeta potential (mV)	Elemental analysis		Charge concentration (mmol/kg cellulose)
		C (%)	H (%)	
CNC-PS	33.24±1	41.63±0.03	6.30±0.09	98.0
CNC-SP	34.46±2	41.59±0.07	6.42±0.01	53.4
CNC-PH	38.86±4	41.53±0.01	6.27±0.05	102.0
CNC-HP	35.28±4	41.50±0.05	6.29±0.13	46.0

that the nanoparticle has moderate dispersibility in water (Hasani et al., 2008; Filson and Dawson-Andoh, 2009). Meanwhile for the element of S and P, there no trace can be detected due to their low amounts and capability limitation of the instrument (minimum sensitivity is 1%). The charge (sulphate and phosphate) concentration was also determined to support the dispersion ability of CNCs. The results indicate that CNCs isolated using phosphoric acid as the first sequence display higher charge concentration as phosphate anion (bivalent) has stronger inhibition than sulphate or chlorine (Baek et al., 2019). The greater amount of charges for the CNC-PH

and CNC-PS can be attributed to the phosphorylation upon first addition and inhibition to dephosphorylate further upon addition of second acid.

In addition, the reported approach has advantages in terms of reducing consumption of phosphoric acid to produce in thermally stable CNC as compared with single acid hydrolysis. In comparison with the reported mild acid hydrolysis methods using organic acids (oxalic, formic acid) and ionic liquids which present broader size distribution of CNC particles (Chen et al., 2016; Shamshina and Abidi, 2021).

4. Conclusion

This study showed a successful production of thermal stable CNC through a controlled mixed acid hydrolysis using 32wt% phosphoric acid combination with a minimal addition of a strong acid 10% H_2SO_4, or 3.7% HCl at a volume substitution of 4:1. This remarks a significant reduction (54%) in comparison with the process with H_3PO_4 alone. The CNC produced using H_3PO_4 in combination with HCl, possess enhanced thermal stability (275–280 °C), dispersibility in water, high production yield and retained crystallinity. The CNCs reported in this study have much more potential as reinforcing agent in polymer nanocomposites and for processing through melt compounding at elevated temperatures. Furthermore, as one of the immediate implications, this mixed acid strategy can be applied in the hydrolysis process of less refined pulp materials which render processability issues at high solid to liquid ratio due to the long fibres.

Declaration of Cmpeting Interest

There are no conflicts to declare.

Acknowledgements

Khairatun Najwa Mohd Amin gratefully acknowledges the Ministry of Higher Education of Malaysia and Universiti Malaysia Pahang for the research fellowship for this study. Pratheep K. Annamalai acknowledges the Queensland Government for the Advance Queensland Research Fellowship (AQRF). The authors gratefully acknowledge the facilities as well as the scientific and technical assistance by the staff (Dr. Isabel C. Morrow) in the Australian Microscopy and Microanalysis Research Facility (AMMRF) at the Centre for Microscopy and Microanalysis (CMM), the University of Queensland.

Supplementary materials

Supplementary material associated with this article can be found, in the online version, at doi:10.1016/j.jobab.2021.12.002.

References

Amin, K.N.M., Amiralian, N., Annamalai, P.K., Edwards, G., Chaleat, C., Martin, D.J., 2016. Scalable processing of thermoplastic polyurethane nanocomposites toughened with nanocellulose. Chem. Eng. J. 302, 406–416.

Annamalai, P.K., Dagnon, K.L., Monemian, S., Foster, E.J., Rowan, S.J., Weder, C., 2014. Water-responsive mechanically adaptive nanocomposites based on styrene-butadiene rubber and cellulose nanocrystals: processing matters. ACS Appl. Mater. Interfaces 6, 967–976.

Baek, J., Wahid-Pedro, F., Kim, K., Kim, K., Tam, K.C., 2019. Phosphorylated-CNC/modified-chitosan nano complexes for the stabilization of Pickering emulsions. Carbohydr. Polym. 206, 520–527.

Bagheriasl, D., Carreau, P.J., Dubois, C., Riedl, B., 2015. Properties of polypropylene and polypropylene/poly(ethylene-co-vinyl alcohol) blend/CNC nanocomposites. Compos. Sci. Technol. 117, 357–363.

Bai, W., Holbery, J., Li, K.C., 2009. A technique for production of nanocrystalline cellulose with a narrow size distribution. Cellulose 16, 455–465.

Bashar, M.M., Zhu, H.E., Yamamoto, S., Mitsuishi, M., 2019. Highly carboxylated and crystalline cellulose nanocrystals from jute fiber by facile ammonium persulfate oxidation. Cellulose 26, 3671–3684.

Beck-Candanedo, S., Roman, M., Gray, D.G., 2005. Effect of reaction conditions on the properties and behavior of wood cellulose nanocrystal suspensions. Biomacromolecules 6, 1048–1054.

Ben Azouz, K., Ramires, E.C., van den Fonteyne, W., El Kissi, N., Dufresne, A., 2012. Simple method for the melt extrusion of a cellulose nanocrystal reinforced hydrophobic polymer. ACS Macro Lett 1, 236–240.

Boerstoel, H., Maatman, H., Westerink, J.B., Koenders, B.M., 2001. Liquid crystalline solutions of cellulose in phosphoric acid. Polymer 42, 7371–7379.

Bondeson, D., Mathew, A., Oksman, K., 2006. Optimization of the isolation of nanocrystals from microcrystalline celluloseby acid hydrolysis. Cellulose 13, 171–180.

Camarero Espinosa, S., Kuhnt, T., Foster, E.J., Weder, C., 2013. Isolation of thermally stable cellulose nanocrystals by phosphoric acid hydrolysis. Biomacromolecules 14, 1223–1230.

Capadona, J.R., van den Berg, O., Capadona, L.A., Schroeter, M., Rowan, S.J., Tyler, D.J., Weder, C., 2007. A versatile approach for the processing of polymer nanocomposites with self-assembled nanofibre templates. Nat. Nanotechnol. 2, 765–769.

Chen, L.H., Wang, Q.Q., Hirth, K., Baez, C., Agarwal, U.P., Zhu, J.Y., 2015. Tailoring the yield and characteristics of wood cellulose nanocrystals (CNC) using concentrated acid hydrolysis. Cellulose 22, 1753–1762.

Chen, L.H., Zhu, J.Y., Baez, C., Kitin, P., Elder, T., 2016. Highly thermal-stable and functional cellulose nanocrystals and nanofibrils produced using fully recyclable organic acids. Green Chem 18, 3835–3843.

Corrêa, A.C., Morais Teixeira, E., Pessan, L.A., Mattoso, L.H.C., 2010. Cellulose nanofibers from curaua fibers. Cellulose 17, 1183–1192.

Dunlop, M.J., Acharya, B., Bissessur, R., 2018. Isolation of nanocrystalline cellulose from tunicates. J. Environ. Chem. Eng. 6, 4408–4412.

Fan, L.H., Lu, Y.Q., Yang, L.Y., Huang, F.F., Ouyang, X.K., 2019. Fabrication of polyethylenimine-functionalized sodium alginate/cellulose nanocrystal/polyvinyl alcohol core-shell microspheres ((PVA/SA/CNC)@PEI) for diclofenac sodium adsorption. J. Colloid Interface Sci. 554, 48–58.

Filson, P.B., Dawson-Andoh, B.E., 2009. Sono-chemical preparation of cellulose nanocrystals from lignocellulose derived materials. Bioresour. Technol. 100, 2259–2264.

Gray, N., Hamzeh, Y., Kaboorani, A., Abdulkhani, A., 2018. Influence of cellulose nanocrystal on strength and properties of low density polyethylene and thermoplastic starch composites. Ind. Crops Prod. 115, 298–305.

Hamdan, M.A., Khairatun Najwa, M.A., Jose, R., Martin, D., Adam, F., 2021. Tuning mechanical properties of seaweeds for hard capsules: a step forward for a sustainable drug delivery medium. Food Hydrocoll. Heal. 1, 100023.
Hasani, M., Cranston, E.D., Westman, G., Gray, D.G., 2008. Cationic surface functionalization of cellulose nanocrystals. Soft Matter 4, 2238–2244.
Hendren, K.D., Baughman, T.W., Deck, P.A., Foster, E.J., 2020. In situ dispersion and polymerization of polyethylene cellulose nanocrystal-based nanocomposites. J. Appl. Polym. Sci. 137, 48500.
Hirayama, J., Kobayashi, H., Fukuoka, A., 2020. Amorphization and semi-dry conversion of crystalline cellulose to oligosaccharides by impregnated phosphoric acid. Bull. Chem. Soc. Jpn. 93, 273–278.
Hosseinmardi, A., Annamalai, P.K., Martine, B., Pennells, J., Martin, D.J., Amiralian, N., 2018. Facile tuning of the surface energy of cellulose nanofibers for nanocomposite reinforcement. ACS Omega 3, 15933–15942.
Jia, X.J., Chen, Y.W., Shi, C., Ye, Y.F., Wang, P., Zeng, X.X., Wu, T., 2013. Preparation and characterization of cellulose regenerated from phosphoric acid. J. Agric. Food Chem. 61, 12405–12414.
Jordan, J.H., Easson, M.W., Dien, B., Thompson, S., Condon, B.D., 2019. Extraction and characterization of nanocellulose crystals from cotton gin motes and cotton gin waste. Cellulose 26, 5959–5979.
Kargarzadeh, H., Ahmad, I., Abdullah, I., Dufresne, A., Zainudin, S.Y., Sheltami, R.M., 2012. Effects of hydrolysis conditions on the morphology, crystallinity, and thermal stability of cellulose nanocrystals extracted from kenaf bast fibers. Cellulose 19, 855–866.
Kupiainen, L., Ahola, J., Tanskanen, J., 2012. Distinct effect of formic and sulfuric acids on cellulose hydrolysis at high temperature. Ind. Eng. Chem. Res. 51, 3295–3300.
Lazko, J., Sénéchal, T., Landercy, N., Dangreau, L., Raquez, J.M., Dubois, P., 2014. Well defined thermostable cellulose nanocrystals via two-step ionic liquid swelling-hydrolysis extraction. Cellulose 21, 4195–4207.
Leszczyńska, A., Radzik, P., Haraźna, K., Pielichowski, K., 2018. Thermal stability of cellulose nanocrystals prepared by succinic anhydride assisted hydrolysis. Thermochimica Acta 663, 145–156.
Li, D., Henschen, J., Ek, M., 2017. Esterification and hydrolysis of cellulose using oxalic acid dihydrate in a solvent-free reaction suitable for preparation of surface–functionalised cellulose nanocrystals with high yield. Green Chem 19, 5564–5567.
Li, W., Yue, J.Q., Liu, S.X., 2012. Preparation of nanocrystalline cellulose via ultrasound and its reinforcement capability for poly(vinyl alcohol) composites. Ultrason. Sonochem. 19, 479–485.
Lin, N., Dufresne, A., 2013. Physical and/or chemical compatibilization of extruded cellulose nanocrystal reinforced polystyrene nanocomposites. Macromolecules 46, 5570–5583.
Mahmud, M.M., Perveen, A., Jahan, R.A., Matin, M.A., Wong, S.Y., Li, X., Arafat, M.T., 2019. Preparation of different polymorphs of cellulose from different acid hydrolysis medium. Int. J. Biol. Macromol. 130, 969–976.
Mendez, J., Annamalai, P.K., Eichhorn, S.J., Rusli, R., Rowan, S.J., Foster, E.J., Weder, C., 2011. Bioinspired mechanically adaptive polymer nanocomposites with water-activated shape-memory effect. Macromolecules 44, 6827–6835.
Miao, C.W., Hamad, W.Y., 2019. Critical insights into the reinforcement potential of cellulose nanocrystals in polymer nanocomposites. Curr. Opin. Solid State Mater. Sci. 23, 100761.
Mohd Amin, K.N., Annamalai, P.K., Morrow, I.C., Martin, D., 2015. Production of cellulose nanocrystals via a scalable mechanical method. RSC Adv 5, 57133–57140.
Molnes, S.N., Paso, K.G., Strand, S., Syverud, K., 2017. The effects of pH, time and temperature on the stability and viscosity of cellulose nanocrystal (CNC) dispersions: implications for use in enhanced oil recovery. Cellulose 24, 4479–4491.
Moon, R.J., Martini, A., Nairn, J., Simonsen, J., Youngblood, J., 2011. Cellulose nanomaterials review: structure, properties and nanocomposites. Chem. Soc. Rev. 40, 3941.
Nagalakshmaiah, M., Nechyporchuk, O, El Kissi, N., Dufresne, A., 2017. Melt extrusion of polystyrene reinforced with cellulose nanocrystals modified using poly [(styrene)-co-(2-ethylhexyl acrylate)] latex particles. Eur. Polym. J. 91, 297–306.
Norrrahim, M.N.F., Nurazzi, N.M., Jenol, M.A., Farid, M.A.A., Janudin, N., Ujang, F.A., Yasim-Anuar, T.A.T., Syed Najmuddin, S.U.F., Ilyas, R.A., 2021. Emerging development of nanocellulose as an antimicrobial material: an overview. Mater. Adv. 2, 3538–3551.
Pei, A.H., Malho, J.M., Ruokolainen, J., Zhou, Q., Berglund, L.A., 2011. Strong nanocomposite reinforcement effects in polyurethane elastomer with low volume fraction of cellulose nanocrystals. Macromolecules 44, 4422–4427.
Rahimi, S.K., Otaigbe, J.U., 2017. The effects of the interface on microstructure and rheo-mechanical properties of polyamide 6/cellulose nanocrystal nanocomposites prepared by *in situ* ring-opening polymerization and subsequent melt extrusion. Polymer 127, 269–285.
Rämänen, P., Penttilä, P.A., Svedström, K., Maunu, S.L., Serimaa, R., 2012. The effect of drying method on the properties and nanoscale structure of cellulose whiskers. Cellulose 19, 901–912.
Reid, M.S., Erlandsson, J., Wågberg, L., 2019. Interfacial polymerization of cellulose nanocrystal polyamide *Janus* nanocomposites with controlled architectures. ACS Macro Lett 8, 1334–1340.
Roman, M., Winter, W.T., 2004. Effect of sulfate groups from sulfuric acid hydrolysis on the thermal degradation behavior of bacterial cellulose. Biomacromolecules 5, 1671–1677.
Roohani, M., Habibi, Y., Belgacem, N.M., Ebrahim, G., Karimi, A.N., Dufresne, A., 2008. Cellulose whiskers reinforced polyvinyl alcohol copolymers nanocomposites. Eur. Polym. J. 44, 2489–2498.
Rosa, M.F., Medeiros, E.S., Malmonge, J.A., Gregorski, K.S., Wood, D.F., Mattoso, L.H.C., Glenn, G., Orts, W.J., Imam, S.H., 2010. Cellulose nanowhiskers from coconut husk fibers: effect of preparation conditions on their thermal and morphological behavior. Carbohydr. Polym. 81, 83–92.
Sadeghifar, H., Filpponen, I., Clarke, S.P., Brougham, D.F., Argyropoulos, D.S., 2011. Production of cellulose nanocrystals using hydrobromic acid and click reactions on their surface. J. Mater. Sci. 46, 7344–7355.
Segal, L., Creely, J.J., Martin Jr, A.E., Conrad, C.M., 1959. An empirical method for estimating the degree of crystallinity of native cellulose using the X-ray diffractometer. Text. Res. J. 29, 786–794.
Shamshina, J.L., Abidi, N., 2021. Cellulose nanocrystals from ionic liquids: a critical review. Green Chem 23, 6205–6222.
Sojoudiasli, H., Heuzey, M.C., Carreau, P.J., 2018. Mechanical and morphological properties of cellulose nanocrystal-polypropylene composites. Polym. Compos. 39, 3605–3617.
Song, X.Y., Zhou, L.J., Ding, B.B., Cui, X., Duan, Y.X., Zhang, J.M., 2018. Simultaneous improvement of thermal stability and redispersibility of cellulose nanocrystals by using ionic liquids. Carbohydr. Polym. 186, 252–259.
Sperotto, G., Stasiak, L.G., Godoi, J.P.M.G., Gabiatti, N.C., de Souza, S.S., 2021. A review of culture media for bacterial cellulose production: complex, chemically defined and minimal media modulations. Cellulose 28, 2649–2673.
Sun, Y., Lin, L., Deng, H.B., Peng, H., Li, J.Z., Sun, R.C., Liu, S.J., 2008. Hydrolysis of bamboo fiber cellulose in formic acid. Front. For. China 3, 480–486.
Tang, L.R., Huang, B., Ou, W., Chen, X.R., Chen, Y.D., 2011. Manufacture of cellulose nanocrystals by cation exchange resin-catalyzed hydrolysis of cellulose. Bioresour. Technol. 102, 10973–10977.
Vanderfleet, O.M., Reid, M.S., Bras, J., Heux, L., Godoy-Vargas, J., Panga, M.K.R., Cranston, E.D., 2019. Insight into thermal stability of cellulose nanocrystals from new hydrolysis methods with acid blends. Cellulose 26, 507–528.
Viet, D., Beck-Candanedo, S., Gray, D.G., 2007. Dispersion of cellulose nanocrystals in polar organic solvents. Cellulose 14, 109–113.
Vinogradov, V.V., Mizerovskii, L.N., Akaev, O.P., 2002. Reaction of cellulose with aqueous solutions of orthophosphoric acid. Fibre Chem 34, 167–171.
Wang, N., Ding, E.Y., Cheng, R.S., 2007. Thermal degradation behaviors of spherical cellulose nanocrystals with sulfate groups. Polymer 48, 3486–3493.
Wei, S., Kumar, V., Banker, G.S., 1996. Phosphoric acid mediated depolymerization and decrystallization of cellulose: preparation of low crystallinity cellulose—A new pharmaceutical excipient. Int. J. Pharm. 142, 175–181.
Xie, H.X., Zou, Z.F., Du, H.S., Zhang, X.Y., Wang, X.M., Yang, X.H., Wang, H., Li, G.B., Li, L., Si, C.L., 2019. Preparation of thermally stable and surface-functionalized cellulose nanocrystals via mixed H_2SO_4/Oxalic acid hydrolysis. Carbohydr. Polym. 223, 115116.

Yu, H.Y., Abdalkarim, S.Y.H., Zhang, H., Wang, C., Tam, K.C., 2019. Simple process to produce high-yield cellulose nanocrystals using recyclable citric/hydrochloric acids. ACS Sustainable Chem. Eng. 7, 4912–4923.
Yu, H.Y., Qin, Z.Y., Liang, B.L., Liu, N., Zhou, Z., Chen, L., 2013. Facile extraction of thermally stable cellulose nanocrystals with a high yield of 93% through hydrochloric acid hydrolysis under hydrothermal conditions. J. Mater. Chem. A 1, 3938.
Yue, Y.Y., Zhou, C.J., French, A.D., Xia, G., Han, G.P., Wang, Q.W., Wu, Q.L., 2012. Comparative properties of cellulose nano-crystals from native and mercerized cotton fibers. Cellulose 19, 1173–1187.
Zhang, J.H., Zhang, J.Q., Lin, L., Chen, T.M., Zhang, J., Liu, S.J., Li, Z.J., Ouyang, P.K., 2009. Dissolution of microcrystalline cellulose in phosphoric acid: molecular changes and kinetics. Molecules 14, 5027–5041.
Zhang, Y.H., Cui, J.B., Lynd, L.R., Kuang, L.R., 2006. A transition from cellulose swelling to cellulose dissolution by o-phosphoric acid: evidence from enzymatic hydrolysis and supramolecular structure. Biomacromolecules 7, 644–648.